

# CASE: Contrastive Activation for Saliency Estimation

Dane Williamson, Matthew Dwyer, Yangfeng Ji  
University of Virginia  
Email: {dw3zn, md3cn, yj3fs}@virginia.edu

**Abstract**—Saliency methods are widely used to visualize which input features are deemed relevant to a model’s prediction. However, their visual plausibility can obscure critical limitations. In this work, we propose a diagnostic test for class sensitivity: a method’s ability to distinguish between competing class labels on the same input. Through extensive experiments, we show that many widely used saliency methods produce nearly identical explanations regardless of the class label, calling into question their reliability. We find that class-insensitive behavior persists across architectures and datasets, suggesting the failure mode is structural rather than model-specific. Motivated by these findings, we introduce CASE, a contrastive explanation method that isolates features uniquely discriminative for the predicted class. We evaluate CASE using the proposed diagnostic and a perturbation-based fidelity test, and show that it produces faithful and more class-specific explanations than existing methods.

## I. INTRODUCTION

As deep learning systems become more widely deployed, explanation methods are increasingly relied upon to justify, debug, and evaluate model predictions. Activation-based approaches such as Class Activation Mapping (CAM) [1] and Gradient-Weighted Class Activation Mapping (Grad-CAM) [2] are among the most widely used tools for interpreting convolutional neural networks (CNNs). These methods aim to highlight features in the input that are most relevant to a particular class prediction. However, despite their popularity, such saliency methods often exhibit a critical failure mode: they produce nearly identical explanations for different class labels on the same input. [3], [4]. This redundancy undermines their utility in settings where distinguishing between predictions is essential, such as auditing errors, understanding misclassifications, or building trust in model behavior. [5]–[9]

This concern is echoed in human-centered studies such as HIVE [10], which show that visual explanations can increase user trust even when the model is wrong, raising the risk that visually plausible but semantically empty saliency maps may mislead stakeholders. They also observe that existing methods often produce indistinguishable explanations for correct and incorrect predictions, suggesting a broader insensitivity to class label. In high-stakes applications, such as diagnosis or safety monitoring, this insensitivity directly compromises the value of explanations as a safeguard against error. Notably, real-world failures of saliency methods have been documented in medical imaging, where models mistakenly rely on dataset artifacts, such as text tokens or positional cues, rather than pathology features, leading to clinically misleading saliency maps. [9].

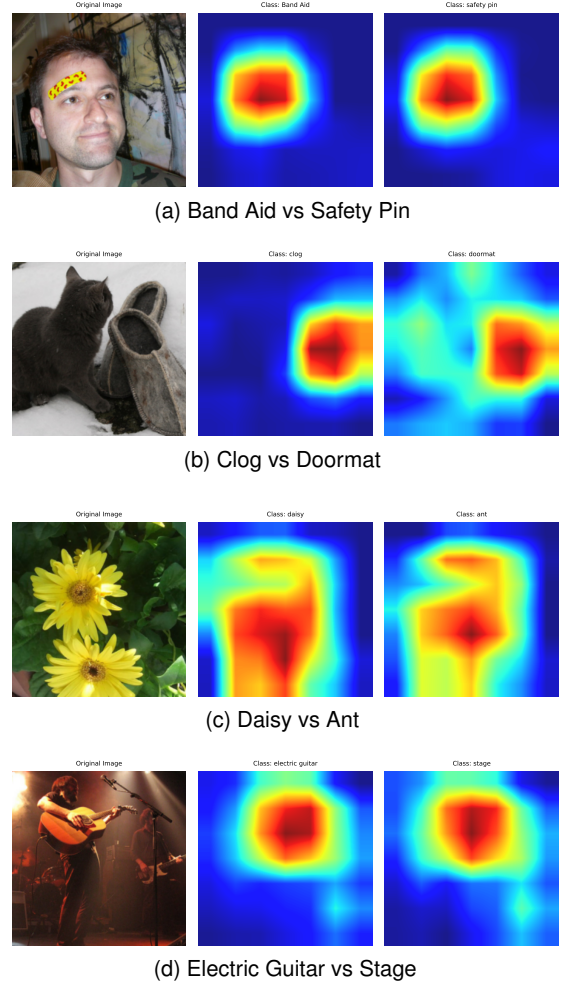


Fig. 1. Saliency maps for different class labels on the same image using Grad-CAM. Despite switching the target class, the highlighted regions remain nearly identical, indicating a lack of class-specificity. This supports our diagnostic findings in RQ1.

Motivated by these concerns, we focus on two essential properties that explanation methods should satisfy in classification settings:

- **Class-Specificity:** Explanations should reflect features that are distinctive to the target class. Saliency maps for semantically disjoint labels (e.g., *airplane* vs. *barbell*) should differ more than those for related ones (e.g., *terrier* vs. *poodle*). Bau et al. [11] demonstrate that CNN units can align with human-interpretable concepts, suggesting that class-specific representations are both learnable and quantifiable.
- **High Fidelity:** Explanations should faithfully reflect the model’s internal reasoning. This is best assessed

through model-grounded metrics, such as confidence change after perturbing salient features. [12]–[15]

To illustrate this issue, Figure 1 compares saliency maps generated for the top-1 and top-2 predicted class labels on the same input. Despite the class label change, methods such as Grad-CAM produce nearly identical explanations, highlighting the same spatial regions. This visual similarity, even between semantically distinct classes, suggests that many popular saliency methods fail to isolate class-discriminative evidence.

We formalize this observation as a diagnostic test for class sensitivity. Specifically, we compute the top- $k$  feature overlap between saliency maps generated for different class labels on the same input. A method that highlights the same regions regardless of label fails this test. We evaluate this behavior using a one-sided Wilcoxon signed-rank test to assess whether the median agreement exceeds a lenient threshold. This analysis serves as a model- and method-agnostic check of whether a saliency method distinguishes among competing class hypotheses.

To address the limitation of class-insensitivity, we introduce **CASE** (Contrastive Activation for Saliency Estimation), a contrastive extension of Grad-CAM designed to highlight features that are uniquely discriminative for the target class. CASE compares neuron activations for the predicted class against those of a contrast class, reducing shared attribution and improving class specificity. Importantly, CASE requires no architectural modifications and operates on the internal activations of the trained model.

We evaluate CASE alongside five popular saliency methods across four architectures and two datasets. In our class-sensitivity diagnostic, CASE consistently produces lower top- $k$  overlap between class labels than baseline methods. In a complementary fidelity test, we measure the drop in model confidence after minimally perturbing the top- $k$  salient features. CASE achieves competitive confidence drop, indicating stronger alignment with decision-relevant evidence.

### Contributions.

- 1) We introduce a diagnostic test for class sensitivity that quantifies top- $k$  feature overlap between saliency maps for different class labels on the same input. Applying this test to five widely used saliency methods across four architectures and two datasets, we find that most methods fail to distinguish between competing classes, even for semantically distinct categories.
- 2) We propose CASE, a contrastive saliency method that isolates uniquely discriminative features by subtracting gradient components shared with frequently confused classes. CASE consistently produces more class-specific saliency maps and maintains strong attribution fidelity, outperforming baselines on class sensitivity and matching them on faithfulness.

## II. RELATED WORK

### A. Contrastive Explanations

A number of prior methods have explored contrastive reasoning to enhance interpretability. CWOX [16] formulates

explanation as a clustering problem over confusion sets, requiring class-specific explanations to differ from those of their nearest neighbors in a latent tree. While conceptually appealing, CWOX relies on HLTA-derived cluster structures and explicit contrast baselines, which may introduce brittleness or restrict applicability. [17]

Contrastive Layer-wise Relevance Propagation (C-LRP) [18] extends the LRP [19] framework to compare class-specific relevance maps to those of reference classes. However, C-LRP remains tied to backpropagation-based relevance signals and does not extend to activation-based methods like CAM.

In contrast, our approach introduces a contrastive mechanism within the CAM framework, leveraging natural competition between class logits to isolate class-discriminative evidence. We avoid the need for external baselines or learned structures, focusing instead on intrinsic class separability within the model’s own prediction space.

### B. Saliency Methods and Class Insensitivity

Grad-CAM [2] and its variants (e.g., Grad-CAM++ [20], AblationCAM [21], ScoreCAM [22], LayerCAM [23]) have become standard tools for visualizing model predictions. These methods produce spatial heatmaps based on either gradient or activation weighting. However, several studies have highlighted their limitations with respect to faithfulness and class sensitivity.

Adebayo et al. [24] demonstrate that certain saliency methods are invariant to randomization of model weights or labels, failing what they term “*sanity checks*.” Their work introduces the notion of *model-insensitivity*, where attribution maps remain unchanged even as the model parameters are randomized. While this critique reveals concerning invariance patterns, it targets *variation across models*, not *across class predictions within the same model*.

In contrast, our work focuses on a different failure mode: *class-insensitivity*. We show that many activation-based methods produce nearly identical saliency maps for different class labels<sup>1</sup>, suggesting they fail to isolate discriminative evidence. This form of insensitivity undermines the explanatory value of class-conditional attribution. While later variants of Grad-CAM improve visual smoothness or localization, they do not resolve this overlap in class-specific evidence. Our method addresses this by introducing a contrastive correction based on internal class competition, directly targeting the class-indistinct attribution problem.

### C. Discriminative Features and Exclusivity

Beyond attribution intensity, several works have investigated the exclusivity of features with respect to class labels. Kalibhat et al. [25] define discriminative features as those with positive gradient contributions toward a class score:

$$D_c = \left\{ a \in A \mid \frac{\partial y^c}{\partial a} > 0 \right\} \quad (1)$$

<sup>1</sup>see Figure 1

However, such features may overlap across classes, i.e.,  $\exists c \neq c' : D_c \cap D_{c'} \neq \emptyset$ , leading to ambiguity. This reflects a fundamental limitation of gradient-based attribution: it reveals support, but not necessarily specificity. Our work explicitly targets this gap, focusing on isolating features that are not just correlated with the target class, but uniquely discriminative relative to plausible alternatives.

#### D. Agreement Metrics and Evaluation of Saliency

Several metrics have been proposed to evaluate saliency maps based on consistency and selectivity. Krishna et al. [26] introduce the notion of the *disagreement problem*, observing that saliency maps for different class labels often highlight overlapping regions. They propose overlap-based metrics to assess class-separability in explanations. We adopt and extend this framework by applying the Wilcoxon signed-rank test to determine whether saliency methods systematically fail to distinguish between top-1 and top-2 predictions. This offers a statistical lens on class sensitivity that complements visual inspection.

#### E. Summary

In summary, while prior work has surfaced critical limitations of saliency methods, such as insensitivity to model or data [24], or failure to isolate class-specific features [25], [26], few methods provide both class-distinctiveness and architectural compatibility. Our work addresses this gap by quantifying class overlap in existing methods and introducing a contrastive refinement tailored to activation-based explanations. This yields clearer, more class-sensitive visualizations and aligns explanatory focus with the model’s internal decision boundaries.

### III. CONTRASTIVE ACTIVATION FOR SALIENCY ESTIMATION (CASE)

#### A. Overview

We introduce **CASE** (Contrastive Activation for Saliency Estimation), a gradient-based saliency method designed to improve class-specificity by suppressing shared attribution between frequently confused class labels. While existing saliency methods highlight features that contribute to a class prediction, they often fail to distinguish between closely related classes, yielding nearly identical explanations across labels. CASE addresses this by explicitly removing gradient components shared with a contrast set, classes that the model confuses with the target, thereby isolating uniquely discriminative evidence. The full procedure is detailed in Algorithm 1 and visualized in Figure 2.

#### B. Contrastive Gradients

Prior work has observed that many saliency methods produce overlapping explanations across distinct class labels [26], limiting their ability to convey what distinguishes one class from another. In CASE, we begin by computing the gradient of the class score  $s_u$  with respect to the activation map  $A$  for the target class  $u$ . We then suppress the components

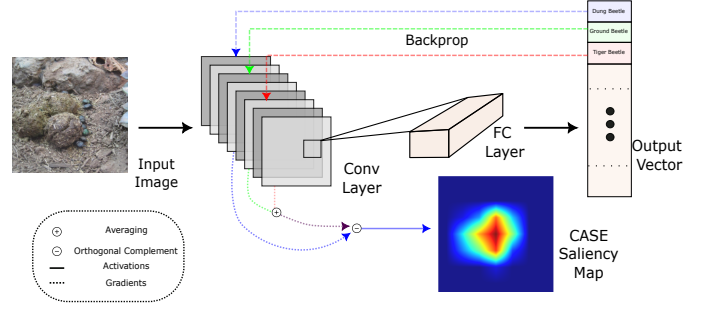


Fig. 2. Overview of the CASE algorithm. Gradients are backpropagated for the target class (blue) and contrast classes (red, green). The contrast gradients are averaged, and the target gradient is projected onto this average. The projection is then subtracted from the original target gradient to isolate a class-specific signal. The resulting orthogonal component is used to compute the weights for the final saliency map.

of this gradient that are aligned with an average gradient vector derived from a contrast set, i.e., the classes most frequently confused with  $u$ . This orthogonalization removes shared attribution directions and emphasizes features that are uniquely predictive of  $u$ .

#### C. Confusion-Based Contrast Set Selection

To identify an appropriate contrast set, CASE uses the model’s confusion matrix  $M \in \mathbb{R}^{C \times C}$ , computed on a held-out validation set. For a given class  $u$ , we extract the top- $k$  most confused alternatives:

$$\mathcal{V} = \arg \max_{v \in C \setminus \{u\}}^k M[u, v] \quad (2)$$

This behaviorally grounded approach ensures that the contrast set  $\mathcal{V}$  consists of labels that the model empirically struggles to distinguish from  $u$ , rather than relying on semantic priors or embedding similarity. The mean gradient across this set is used to define a shared attribution direction to suppress.

#### D. Uniquely Discriminative Features

Let  $D_u$  denote the set of features positively contributing to class  $u$ , and let  $D_v$  represent those for a contrast class  $v \in \mathcal{V}$ . The goal of CASE is to approximate the uniquely discriminative feature set:

$$U_u^{\mathcal{V}} = D_u \setminus \bigcup_{v \in \mathcal{V}} D_v \quad (3)$$

By suppressing attribution that overlaps with the contrast set, CASE highlights only those features that are uniquely predictive of the target class. For example, distinguishing *tiger shark* from *great white shark* involves removing marine features common to both, while retaining subtle class-specific traits.

#### E. Saliency Map Generation

To construct the final saliency map, CASE computes the orthogonal projection of the target gradient  $\gamma_u = \nabla_{A s_u}$  against the average contrast gradient  $\bar{\gamma}$ , where:

---

**Algorithm 1** CASE with Confusion-Based Contrast
 

---

- 1: **Input:** Bottleneck activation maps  $A \in \mathbb{R}^{N \times H \times W}$ ; Confusion matrix  $M \in \mathbb{R}^{C \times C}$ ; Target class  $u \in C$ ; Number of contrast classes  $k$ ; Upsampling factor  $\beta$
- 2: **Output:** Saliency map  $S \in \mathbb{R}^{H \times W}$
- 3: Compute target gradient:  $\gamma_u = \nabla_A s_u$
- 4: Identify top- $k$  confused classes:

$$\mathcal{V} = \arg \max_{v \in C \setminus \{u\}} M[u, v]$$

- 5: Initialize contrast gradient accumulator:  $\bar{\gamma} = 0$
- 6: **for** each  $v \in \mathcal{V}$  **do**
- 7:    $\gamma_v = \nabla_A s_v$
- 8:    $\bar{\gamma} += \gamma_v$
- 9: **end for**
- 10:  $\bar{\gamma} /= k$  // Mean contrast gradient
- 11: Project  $\gamma_u$  onto orthogonal complement of  $\bar{\gamma}$ :

$$\gamma_u^\perp = \gamma_u - \frac{\langle \gamma_u, \bar{\gamma} \rangle}{\|\bar{\gamma}\|^2 + \epsilon} \cdot \bar{\gamma}$$

- 12: Compute saliency:

$$S = (\max \{ \gamma_u^\perp \cdot A, 0 \}) \uparrow \beta$$


---

$$\bar{\gamma} = \frac{1}{k} \sum_{v \in \mathcal{V}} \nabla_A s_v \quad (4)$$

The projection is given by:

$$\gamma_u^\perp = \gamma_u - \frac{\langle \gamma_u, \bar{\gamma} \rangle}{\|\bar{\gamma}\|^2 + \epsilon} \cdot \bar{\gamma} \quad (5)$$

This removes shared directional components between  $\gamma_u$  and the contrast set. The resulting class-specific saliency map is computed via a weighted sum over the activation maps and passed through a ReLU and upsampling step:

$$S = (\text{ReLU} [\gamma_u^\perp \cdot A]) \uparrow \beta \quad (6)$$

Here,  $A \in \mathbb{R}^{C \times H \times W}$  denotes the final convolutional activation tensor, and  $\uparrow \beta$  indicates bilinear upsampling to input resolution. This formulation yields saliency maps that emphasize evidence uniquely associated with the predicted class and suppress attribution that generalizes across visually similar alternatives.

#### IV. EXPERIMENTS

This section presents our empirical evaluation of saliency method performance with a focus on class sensitivity and explanation faithfulness. We structure our analysis around two guiding research questions.

##### A. Research Questions

**RQ1: How does CASE compare to existing saliency methods in isolating class-specific evidence across architectures?**

**RQ2: Can CASE improve class sensitivity without compromising explanation fidelity?**

##### B. RQ1: Class Sensitivity

RQ1 aims to determine whether saliency methods meaningfully distinguish between class labels when generating explanations for the same input. For each image, we generate saliency maps using the top-1 and top-2 predicted class labels and compute the overlap between their top- $k$  most salient pixels. High overlap would indicate that a method tends to highlight the same regions regardless of class label, suggesting poor class sensitivity.

To quantify this behavior, we use the feature agreement metric proposed by [26], which computes the proportion of shared features among the top- $k$  salient pixels:

$$F(E, E', k) = \frac{|\{f : f \in t(E, E', k)\}|}{k} \quad (7)$$

where  $E$  and  $E'$  are saliency maps for two different class labels, and  $t(E, E', k)$  returns the intersection of the top- $k$  salient features for both.

We compute this score across a large sample of validation images for each method. A one-sided Wilcoxon signed-rank test is then applied to assess whether the observed agreement scores are significantly lower than would be expected under class-insensitive behavior.

The null hypothesis is that the median agreement between saliency maps for the top-1 and top-2 class labels is greater than or equal to 50%. A statistically significant rejection of this hypothesis indicates that the method produces class-distinct explanations.

$$\begin{aligned} H_0 : & \text{Median}(F(E, E', k)) \geq 0.50 \\ H_1 : & \text{Median}(F(E, E', k)) < 0.50 \end{aligned} \quad (8)$$

##### C. RQ2: Explanation Faithfulness

RQ2 evaluates whether CASE produces more faithful saliency maps compared to baseline methods. We define explanation faithfulness as the degree to which the most salient regions identified by a method correspond to regions truly influential to the model's prediction.

To measure this, we ablate the top- $k$  most salient regions identified by each method and observe the resulting drop in classification confidence for the predicted class. Larger confidence drops indicate that the identified regions were more influential to the model's decision, and therefore reflect greater faithfulness.

We compute the confidence drop for each method across the same set of evaluation samples and apply a paired t-test to compare CASE against each baseline. This enables a controlled comparison of attribution fidelity while accounting for variability across inputs.

The null hypothesis is that the mean confidence drop from ablating CASE's top- $k$  salient regions is less than or equal to the mean drop from the baseline method. Rejection of this hypothesis indicates that CASE produces significantly more faithful explanations.

$$\begin{aligned} H_0 : & \text{Mean}(D_{\text{CASE}}) \leq \text{Mean}(D_{\text{baseline}}) \\ H_1 : & \text{Mean}(D_{\text{CASE}}) > \text{Mean}(D_{\text{baseline}}) \end{aligned} \quad (9)$$

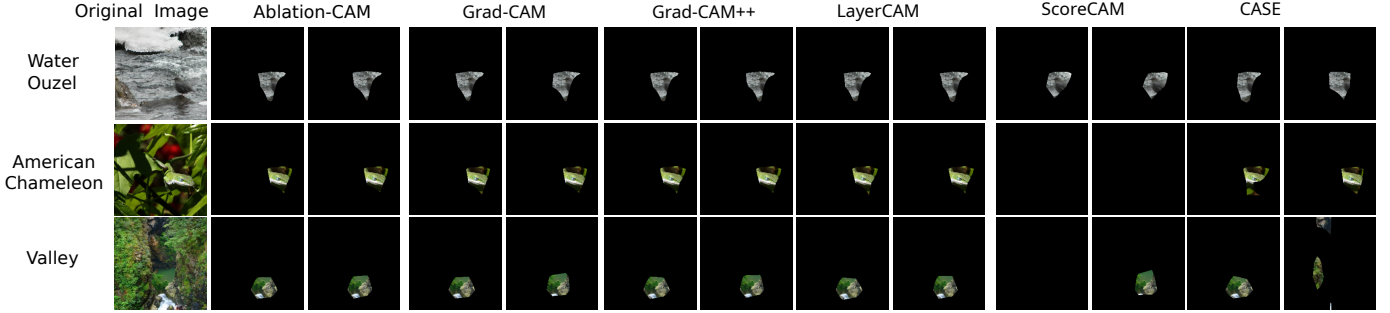


Fig. 3. Class sensitivity comparison across saliency methods. Each row shows the original image and saliency-based feature masking for the top 5 % of the most salient pixels for the top-2 predicted classes. The methods compared are Grad-CAM, Grad-CAM++, ScoreCAM, AblationCAM, LayerCAM, and CASE. For each method, the left masked output corresponds to the most probable class, and the right to the second-most probable class. Row 1: *Water ouzel* vs. *Oystercatcher*; Row 2: *Green lizard* vs. *American chameleon*; Row 3: *Valley* vs. *Cliff*. Methods like ScoreCAM often produce visually identical or absent explanations, highlighting a lack of class-specificity. In contrast, CASE consistently isolates distinct evidence for each class label.

#### D. Models, Datasets, and Methods

Our evaluation includes four pre-trained image classification models: ResNet-50, VGG-19, DenseNet-201, and ConvNeXt-Large [27]–[29]. Models are evaluated on two standard datasets: ImageNet [30], which offers broad category diversity across 1,000 classes, and CIFAR-100 [31], which contains 100 object categories drawn from 20 coarse-grained superclasses. CIFAR-100 consists of low-resolution natural images ( $32 \times 32$ ) covering a wide range of everyday concepts such as animals, vehicles, and household objects.

For each model and dataset, we randomly sample 1000 validation images, retaining only those for which the top-1 prediction is correct. All models are evaluated using publicly available pretrained model without fine-tuning.<sup>2</sup>

We compare CASE against six representative saliency methods: Grad-CAM, Grad-CAM++, Score-CAM, Ablation-CAM, and LayerCAM. Each method is applied using standard configurations with a shared backbone to ensure consistency. All evaluation procedures are applied identically across methods.

### V. RESULTS

#### A. Class Sensitivity Analysis

To evaluate whether existing saliency methods produce class-sensitive explanations, we compute the top-5% feature agreement between saliency maps for the top-1 and top-2 predicted classes on the same input image. High agreement implies that the method highlights largely the same features regardless of the target class, violating the class-specificity criterion.

To complement the quantitative results, Figure 3 presents a visual comparison of masked saliency regions across methods. For each input, we show the masked top-1 and top-2 class explanations produced by Grad-CAM variants, ScoreCAM, LayerCAM, and CASE on a ResNet model. Methods like ScoreCAM and Grad-CAM produce visually indistinct explanations across labels, whereas CASE consistently isolates class-specific evidence.

We perform this analysis across two benchmark datasets (ImageNet and CIFAR-100) and four popular convolutional

TABLE I  
WILCOXON SIGNED-RANK TEST  $p$ -VALUES FOR TOP-5% AGREEMENT BETWEEN SALIENCY MAPS OF TOP-1 AND TOP-2 PREDICTED CLASS LABELS. MODELS ARE PRETRAINED ON IMAGENET. NULL HYPOTHESIS: MEDIAN AGREEMENT  $\geq 50\%$ . BOLDED ENTRIES INDICATE SIGNIFICANT REJECTION OF THE NULL AT  $p < 0.05$ .

Method	ConvNeXt	DenseNet	ResNet	VGG
AblationCAM	1.	< .0001	1.	1.
CASE	< .0001	< .0001	< .0001	< .0001
Grad-CAM	0.8734	< .0001	1.	1.
Grad-CAM++	0.0179	< .0001	1.	< .0001
LayerCAM	< .0001	< .0001	1.	1.
ScoreCAM	< .0001	< .0001	< .0001	1.

architectures (ResNet, DenseNet, VGG, ConvNeXt). For each method–model–dataset combination, we run a one-sided Wilcoxon signed-rank test to evaluate the null hypothesis that the median agreement is greater than or equal to 50%. A statistically significant rejection of the null ( $p < 0.05$ ) indicates that the method produces class-distinct explanations in that setting.

Table I reports the  $p$ -values. For each entry, if  $p < 0.05$ , we reject the null hypothesis and conclude that the method produces significantly different saliency maps for the top-1 and top-2 class labels. If  $p \geq 0.05$ , we fail to reject the null and cannot conclude that the explanations differ.

Across all architectures, CASE consistently rejects the null hypothesis with high confidence ( $p < 0.0001$ ), demonstrating robust class sensitivity. ScoreCAM also performs well on most models but fails on VGG. In contrast, traditional methods like Grad-CAM and AblationCAM frequently fail to distinguish between top-1 and top-2 saliency maps, especially on ResNet and VGG. Interestingly, DenseNet stands out as the most sensitive architecture: nearly all methods, even weak baselines, achieve significance. These trends support the claim that DenseNet’s internal representations are more class-discriminative, and highlight that CASE provides the most consistent and architecture-agnostic signal separation.

1) *Robustness to Training Seeds (DenseNet on CIFAR-100)*: To test whether the class sensitivity observed in DenseNet is robust to training randomness, we retrained DenseNet-201 on CIFAR-100 using five different random seeds. We then re-evaluated the saliency methods using the RQ1 procedure for each independently trained model.

<sup>2</sup>Unless otherwise specified



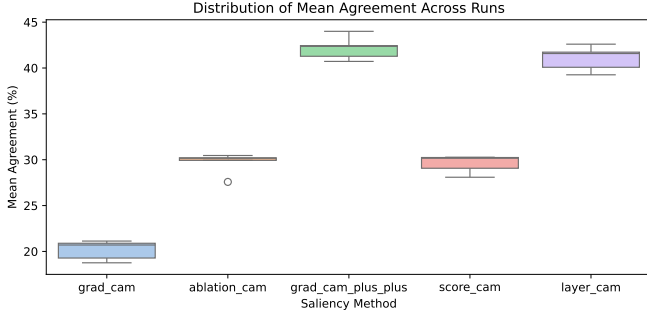


Fig. 4. Mean agreement scores across seeds for each method (DenseNet, CIFAR-100). Lower values indicate more class-distinct saliency.

TABLE II  
RQ1 CLASS SENSITIVITY RESULTS WHEN USING `features.norm5`  
(FINAL NORMALIZATION LAYER) INSTEAD OF THE FINAL  
CONVOLUTIONAL LAYER IN DENSENET-201.

Method	DenseNet (norm5 layer)
AblationCAM	1.
CASE	< 0.0001
Grad-CAM	1.
Grad-CAM++	1.
LayerCAM	1.
ScoreCAM	< 0.0001

As shown in Figure 4, the relative class sensitivity rankings of methods remain consistent across seeds, and all methods continue to reject the null hypothesis. These findings suggest that DenseNet’s ability to produce class-distinct saliency maps is a stable property of the architecture and not an artifact of optimization variability.

### B. Ablation Study: Channel Sparsity and Discriminative Structure

The results in RQ1 reveal that DenseNet exhibits uniquely consistent class sensitivity across saliency methods. To understand this behavior, we analyze the *channel-wise activation patterns* of the layer used for saliency attribution in each architecture.

For each model, we extract activations from the target convolutional layer used in RQ1 and compute the number of channels that are active per input. A channel is considered active if its spatially pooled activation exceeds a small threshold  $\tau$ :

$$\hat{a}_c = \frac{1}{HW} \sum_{i=1}^H \sum_{j=1}^W A_c(i, j), \quad \text{Active if } \hat{a}_c > \tau, \quad (10)$$

where  $A_c$  denotes the activation map for channel  $c$ . For each class, we compute the *mean number of active channels* across correctly predicted validation examples.

We observe a striking pattern in DenseNet. When using  $\tau = 0.001$ , the final convolutional layer (`features.denseblock4.denselayer32.conv2`) exhibits *extremely sparse activation*, averaging fewer than 20 active channels per class. This is in stark contrast to other architectures, whose corresponding attribution layers activate

several hundred channels per class on average. This trend is illustrated in Figure 6, which shows the kernel density estimates (KDE) of mean active channels per class across architectures.

To determine whether this sparsity was a general property of the DenseNet architecture or a consequence of layer selection, we repeated the analysis using an alternative target layer: `features.norm5`, the final batch normalization layer preceding global pooling. As shown in Figure 5, this layer exhibits dramatically higher activation density—nearly all channels are active per class, with the KDE peaking around 1050 channels.

Notably, when we re-ran RQ1 using `features.norm5`, the final normalization layer in DenseNet-201, instead of the final convolutional layer, the results were markedly different. As shown in Table II, most saliency methods failed to reject the null hypothesis, indicating that their explanations did not significantly differ across class labels. This stands in sharp contrast to the results reported in Table I for the convolutional layer, where nearly all methods achieved significant class sensitivity. These findings reinforce the conclusion that saliency quality is highly sensitive to layer choice, and that DenseNet’s class-distinct explanations are driven by the sparse and selective representations encoded in its final convolutional layer. Notably, CASE retains its class sensitivity even under this more diffuse, high-activation regime.

These findings suggest that DenseNet’s final convolutional layer encodes *highly selective and class-discriminative features*. While fewer channels activate, the *identity* of those channels varies meaningfully with class, enabling saliency methods to produce distinct explanations. This aligns with the DenseNet architecture’s design: its dense connectivity may lead to late-stage layers specializing in compact, high-value features with minimal redundancy.

In contrast, architectures like VGG and ConvNeXt exhibit broad activation across many channels, likely reflecting *shared or distributed features* that dilute class-specific signals in the saliency maps. Thus, we posit that *channel-level sparsity coupled with discriminative selectivity* explains why DenseNet supports stronger class-distinct explanations, even when using a layer with minimal activation, whereas dense activation may obscure discriminative attribution.

### C. Explanation Fidelity

To assess the faithfulness of saliency methods, we measure the change in classification confidence after ablating the top- $k$  most salient pixels identified by each method. For each image, we compute the softmax confidence of the predicted class before and after ablation. The difference reflects the influence of the identified regions on the model’s output.

For each method, we compute the average confidence drop and compare it to that of CASE using a paired t-test. The null hypothesis states that the mean confidence drop of the method is greater than or equal to that of CASE. A statistically significant  $p$ -value ( $p < 0.05$ ) supports rejecting the null in favor of the alternative, that CASE yields a higher mean drop.

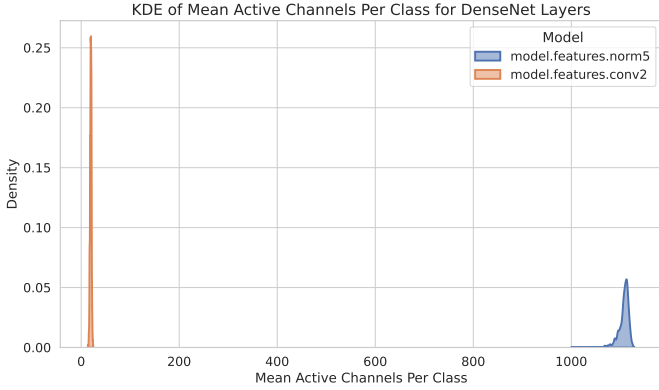


Fig. 5. Kernel density estimate (KDE) of mean active channels per class for two attribution layers in DenseNet-201. The final convolutional layer (`features.denseblock4.denselayer32.conv2`) exhibits extremely sparse activation, with fewer than 20 active channels per class. In contrast, the normalization layer (`features.norm5`) activates nearly all channels. Despite its sparsity, the final convolutional layer yields more class-sensitive saliency maps, underscoring the importance of selecting structurally discriminative layers for attribution.

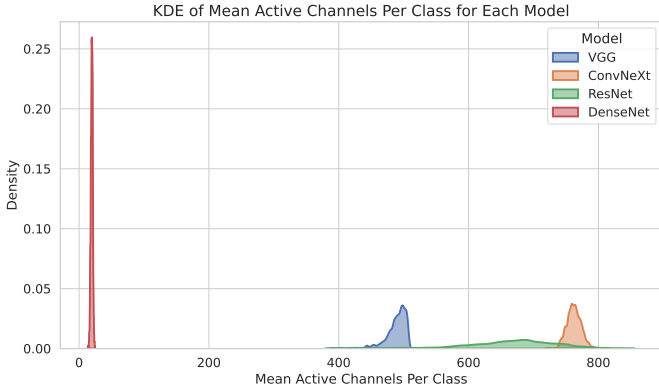


Fig. 6. Distribution of per-class mean active channel counts across architectures. DenseNet shows the most sparse channel activations, with most classes activating fewer than 20 channels. In contrast, ResNet, VGG, and ConvNeXt activate substantially more channels on average.

Table III presents the results across all four architectures. On ConvNeXt, CASE significantly outperforms AblationCAM and LayerCAM, while showing no statistical difference from Grad-CAM, Grad-CAM++, or ScoreCAM. On DenseNet and ResNet, no baseline method differs significantly from CASE, indicating comparable levels of confidence drop. On VGG, three methods, Grad-CAM++, LayerCAM, and ScoreCAM, yield significantly higher drops than CASE, while the remaining methods are not statistically distinguishable.

## VI. DISCUSSION

### A. RQ1: Class Sensitivity of Saliency Methods

The results in Table I demonstrate that the ability of saliency methods to produce class-specific explanations varies substantially across model architectures. DenseNet stands out for its consistent rejection of the null hypothesis across all tested saliency methods, indicating robust class-distinct attribution. In contrast, architectures like VGG and ResNet fail to produce class-sensitive maps under several methods, notably

Grad-CAM and AblationCAM. ScoreCAM achieves broader consistency, performing well on both DenseNet and ResNet, while methods such as LayerCAM and Grad-CAM++ show stronger dependency on the underlying architecture.

These trends suggest that class sensitivity is shaped not only by the saliency algorithm but also by architectural factors. DenseNet’s dense connectivity and feature reuse mechanisms may enable more granular and disentangled activations that preserve class-conditional variation late into the network. However, isolating which architectural features are responsible required targeted ablations.

**Ablation: Robustness to Training Seed Variation:** To test whether the class sensitivity of DenseNet might be a byproduct of training stochasticity, we retrained DenseNet-201 on CIFAR-100 using five random seeds. As shown in Figure 4, the mean agreement distributions across methods remain consistent across all runs. All saliency methods continue to reject the null hypothesis under the RQ1 test, confirming that the class sensitivity is not merely due to favorable initialization but is instead a robust property of the model. This affirms the role of architecture in enabling class-discriminative explanations.

**Ablation: The Role of Layer Selection:** We further investigated whether DenseNet’s class sensitivity could be attributed to the specific layer used for attribution. While conventional practice often selects the final convolutional layer for saliency computation, we found that `features.denseblock4.denselayer32.conv2`, the final convolution in DenseNet-201, exhibited unusually sparse activation. As shown in Figure 6, this layer activates, on average, fewer than 20 channels per class when using a low threshold of  $\tau = 0.001$ , compared to several hundred in VGG, ResNet, and ConvNeXt.

Despite this sparsity, RQ1 results reveal that saliency methods still produce highly class-distinct explanations when using this layer. We interpret this to mean that although few channels are active, their activation patterns are highly class-specific. In other words, DenseNet leverages a compact, selective set of features for each class, which aids saliency methods in isolating discriminative regions.

Importantly, when we re-ran RQ1 using an alternative attribution layer, `features.norm5`, the results were less consistent. Not all methods were able to reject the null hypothesis in this configuration. This shift confirms that layer choice significantly affects explanation quality, even within the same architecture.

While `features.norm5` may appear more appropriate due to its proximity to the classifier and its aggregation of upstream features, our findings reveal that this aggregation may inadvertently homogenize activations across classes. As shown in Figure 5, `norm5` activates nearly all channels uniformly, reducing the saliency method’s ability to isolate class-specific signals. In contrast, the final convolutional layer, though sparsely activated, preserves more localized and class-distinct activation patterns. This highlights a key insight: layers closer to the classifier are not always optimal for attribution, especially when their role is to smooth or normalize a wide range of features. Selective, structurally discriminative layers may offer greater fidelity in class-sensitive explanation tasks.

TABLE III

MEAN CONFIDENCE DROP AND STANDARD DEVIATION AFTER ABATING THE TOP- $k$  SALIENT PIXELS FOR EACH METHOD ON FOUR ARCHITECTURES. HIGHER DROP IMPLIES GREATER ATTRIBUTION FAITHFULNESS.  $p$ -VALUES ARE FROM PAIRED T-TESTS COMPARING EACH METHOD TO CASE (PER MODEL); BOLDED VALUES INDICATE THE HIGHEST MEAN CONFIDENCE DROP FOR A GIVEN MODEL.

Method	ConvNeXt			DenseNet			ResNet			VGG		
	Mean	SD	$p$	Mean	SD	$p$	Mean	SD	$p$	Mean	SD	$p$
AblationCAM	.1696	.2409	.00568	.1140	.2272	.65943	.1339	.2532	.21707	.1354	.2473	.51132
<b>CASE</b>	.2052	.3042	–	.1163	.2274	–	<b>.1411</b>	.2561	–	.1317	.2420	–
Grad-CAM	.1919	.2758	.3544	.1131	.2226	.53783	.136	.2501	.37022	.1328	.2433	.84450
Grad-CAM++	.1872	.286	.22602	.1244	.2417	.13240	.1395	.2584	.78072	.1020	.2096	< .0001
LayerCAM	.1686	.2783	.00988	<b>.1248</b>	.2393	.10838	.1405	.2603	.92128	<b>.1539</b>	.2650	< .0001
ScoreCAM	<b>.2059</b>	.3104	.9665	<b>.1248</b>	.2366	.10598	.1349	.2536	.28969	.1473	.2590	.00645

The ablation in Table II underscores that effective attribution depends not only on proximity to the classifier, but also on the structural selectivity of the chosen layer. These results motivate the need to treat attribution layer selection as a principled design decision, rather than a fixed convention.

*Analysis: Consistency of CASE Across Architectures:* Notably, CASE is the only method that consistently rejects the null hypothesis across all four model architectures in RQ1. This consistency is especially striking on VGG and ResNet, where most traditional methods fail to distinguish between class labels. While ScoreCAM and Grad-CAM++ perform well on specific models, their sensitivity is not uniformly observed. In contrast, CASE provides a robust, architecture-agnostic mechanism for isolating class-specific evidence.

This consistent class sensitivity suggests that the contrastive subtraction in CASE effectively suppresses overlapping or shared attribution components, allowing more discriminative features to emerge, even in architectures where representations are otherwise more entangled. Specifically, CASE operates by isolating a refined subset of the discriminative feature set  $D_u$  (Equation 1) by subtracting the shared components identified in contrast classes  $\mathcal{V}$  (Equation 2). This process approximates the uniquely discriminative feature set  $U_u^{\mathcal{V}}$  (Equation 3), which excludes any features that also support confused alternatives. The effectiveness of this subtraction is evidenced by CASE’s consistent rejection of the null in RQ1, even on architectures where other methods fail. Importantly, this performance is achieved without architecture-specific tuning or structural assumptions, indicating that CASE generalizes well across different model types.

Together, these ablations support the following main findings:

- **Layer selection is critical:** The choice of attribution layer strongly determines whether saliency maps are class-specific. Even within the same model, different layers can produce radically different results under RQ1.
- **Channel activity analysis is diagnostic:** Measuring mean active channels per class reveals which layers exhibit class-variant structure. Sparse but selective layers, like DenseNet’s final convolution, are particularly effective for producing distinct saliency maps.
- **CASE yields robust class sensitivity:** Unlike other methods, CASE consistently produces class-distinct explanations across architectures, underscoring the effectiveness of its contrastive formulation.

## B. RQ2: Explanation Fidelity of Saliency Methods

The results in Table III indicate that CASE achieves statistically significant confidence drops compared to AblationCAM and LayerCAM on ConvNeXt, and performs comparably to the strongest baselines on DenseNet and ResNet. On VGG, several methods: Grad-CAM++, LayerCAM, and ScoreCAM, achieve higher confidence drops than CASE, though only Grad-CAM++ and LayerCAM are significant.

These findings suggest that CASE performs on par with the most widely used attribution methods overall, while providing substantial improvements over weaker baselines. However, attribution fidelity, as measured by the drop in confidence when salient regions are masked, does not always align with class sensitivity. A method may highlight features that are distinct across classes (indicating high RQ1 sensitivity), yet some of these features may exert less influence on the model’s output confidence than shared, highly activated regions. As a result, saliency maps that emphasize uniquely discriminative features may yield relatively modest confidence drops, even if they are more class-specific and interpretable.

Conversely, saliency methods that emphasize broadly activated or background regions may achieve larger confidence drops when those areas are occluded, despite failing to differentiate between classes. This illustrates a key tension: optimizing for overall model confidence may sometimes come at the cost of specificity, and vice versa.

The combined results from RQ1 and RQ2 suggest that CASE addresses a major limitation of existing methods, class-insensitivity, without sacrificing attribution fidelity. While it does not uniformly outperform other methods in confidence drop, its consistently high class specificity represents a complementary strength. This tradeoff makes CASE a valuable addition to the saliency toolbox, particularly in applications that demand clear differentiation between competing class explanations.

## VII. CONCLUSION AND FUTURE DIRECTIONS

We presented CASE, a contrastive activation-based saliency method that isolates class-specific signals by suppressing attribution shared with competing labels. Unlike conventional CAM-style techniques, CASE consistently generates visual explanations that are more class-distinct and aligned with the model’s internal decision-making.

To validate this, we introduced a diagnostic framework for measuring class sensitivity via top- $k$  feature agreement,



and assessed explanation fidelity through confidence drop analysis. Across models and datasets, CASE outperforms or matches existing methods in class specificity and attribution faithfulness.

Our findings also highlight the overlooked influence of architectural features, such as activation sparsity and layer selectivity, on the quality of visual explanations. These insights suggest that saliency methods and model design should be considered jointly, not in isolation.

Future work will focus on adaptive strategies for selecting contrast classes, optimizing runtime, and extending CASE to more complex tasks like multi-label classification and multi-modal reasoning. Ultimately, we see CASE as a step toward saliency methods that not only visualize what a model sees, but explain what truly sets its decisions apart.

## VIII. LIMITATIONS

### *Formulation Constraints*

While CASE improves class sensitivity and attribution fidelity, several limitations remain. First, the method relies on selecting contrastive classes using a confusion matrix, which assumes stable and non-overlapping class relationships. This assumption may break down in low-data regimes or highly imbalanced classification settings. Second, CASE operates on a pairwise contrast between the top-1 prediction and a single contrast class. Extending the formulation to support multi-class or soft-weighted contrast could provide more comprehensive attribution, but this direction remains unexplored.

### *Evaluation Constraints*

Finally, our evaluation is limited to image classification tasks with a single ground-truth label. It is unclear how CASE generalizes to more complex settings such as multi-label classification, hierarchical taxonomies, or vision-language models, where class-conditioned reasoning may involve richer semantics and structured dependencies.

*Computational Overhead:* While CASE introduces minimal architectural dependencies, it incurs additional computational cost relative to standard CAM methods. This is primarily due to the need to compute gradients with respect to multiple contrast classes and perform vector projections at inference time. The added cost scales with the number of contrastive classes  $k$ , although in practice we find that small values (e.g.,  $k = 3$ ) suffice for strong performance. Optimizing the gradient computation pipeline and exploring approximation strategies (e.g., gradient caching or subspace projection) are potential directions for reducing runtime overhead in future deployments.

## PREPRINT NOTICE

This work is currently under review at IEEE Transactions on Neural Networks and Learning Systems (TNNLS).

## REFERENCES

- [1] B. Zhou, A. Khosla, À. Lapedriza, A. Oliva, and A. Torralba, "Learning deep features for discriminative localization," *CoRR*, vol. abs/1512.04150, 2015. [Online]. Available: <http://arxiv.org/abs/1512.04150>
- [2] R. R. Selvaraju, A. Das, R. Vedantam, M. Cogswell, D. Parikh, and D. Batra, "Grad-cam: Why did you say that? visual explanations from deep networks via gradient-based localization," *CoRR*, vol. abs/1610.02391, 2016. [Online]. Available: <http://arxiv.org/abs/1610.02391>
- [3] S. Hooker, D. Erhan, P.-J. Kindermans, and B. Kim, "A benchmark for interpretability methods in deep neural networks," in *Advances in Neural Information Processing Systems*, H. Wallach, H. Larochelle, A. Beygelzimer, F. d'Alché-Buc, E. Fox, and R. Garnett, Eds., vol. 32. Curran Associates, Inc., 2019. [Online]. Available: [https://proceedings.neurips.cc/paper\\_files/paper/2019/file/fe4b8556000d0f0cae99daa5c5c5a410-Paper.pdf](https://proceedings.neurips.cc/paper_files/paper/2019/file/fe4b8556000d0f0cae99daa5c5c5a410-Paper.pdf)
- [4] M. A. A. K. Jalwana, N. Akhtar, M. Bennamoun, and A. Mian, "CAMERAS: enhanced resolution and sanity preserving class activation mapping for image saliency," *CoRR*, vol. abs/2106.10649, 2021. [Online]. Available: <https://arxiv.org/abs/2106.10649>
- [5] A. Alqaraawi, M. Schuessler, P. Weiß, E. Costanza, and N. Berthouze, "Evaluating saliency map explanations for convolutional neural networks: a user study," in *Proceedings of the 25th International Conference on Intelligent User Interfaces*, ser. IUI '20. New York, NY, USA: Association for Computing Machinery, 2020, p. 275–285. [Online]. Available: <https://doi.org/10.1145/3377325.3377519>
- [6] H. Lakkaraju, E. Kamar, R. Caruana, and J. Leskovec, "Faithful and customizable explanations of black box models," in *Proceedings of the 2019 AAAI/ACM Conference on AI, Ethics, and Society*, ser. AIES '19. New York, NY, USA: Association for Computing Machinery, 2019, p. 131–138. [Online]. Available: <https://doi.org/10.1145/3306618.3314229>
- [7] I. Lage, E. Chen, J. He, M. Narayanan, B. Kim, S. Gershman, and F. Doshi-Velez, "An evaluation of the human-interpretability of explanation," *CoRR*, vol. abs/1902.00006, 2019. [Online]. Available: <http://arxiv.org/abs/1902.00006>
- [8] S. Mohseni, N. Zarei, and E. D. Ragan, "A multidisciplinary survey and framework for design and evaluation of explainable ai systems," *ACM Trans. Interact. Intell. Syst.*, vol. 11, no. 3–4, Sep. 2021. [Online]. Available: <https://doi.org/10.1145/3387166>
- [9] E. Tjoa and C. Guan, "A survey on explainable artificial intelligence (xai): Toward medical xai," *IEEE Transactions on Neural Networks and Learning Systems*, vol. 32, no. 11, pp. 4793–4813, 2021.
- [10] S. S. Y. Kim, N. Meister, V. V. Ramaswamy, R. Fong, and O. Russakovsky, "HIVE: evaluating the human interpretability of visual explanations," *CoRR*, vol. abs/2112.03184, 2021. [Online]. Available: <https://arxiv.org/abs/2112.03184>
- [11] D. Bau, B. Zhou, A. Khosla, A. Oliva, and A. Torralba, "Network dissection: Quantifying interpretability of deep visual representations," *CoRR*, vol. abs/1704.05796, 2017. [Online]. Available: <http://arxiv.org/abs/1704.05796>
- [12] W. Samek, A. Binder, G. Montavon, S. Bach, and K. Müller, "Evaluating the visualization of what a deep neural network has learned," *CoRR*, vol. abs/1509.06321, 2015. [Online]. Available: <http://arxiv.org/abs/1509.06321>
- [13] V. Petsiuk, A. Das, and K. Saenko, "RISE: randomized input sampling for explanation of black-box models," *CoRR*, vol. abs/1806.07421, 2018. [Online]. Available: <http://arxiv.org/abs/1806.07421>
- [14] C. Chang, E. Creager, A. Goldenberg, and D. Duvenaud, "Explaining image classifiers by adaptive dropout and generative in-filling," *CoRR*, vol. abs/1807.08024, 2018. [Online]. Available: <http://arxiv.org/abs/1807.08024>
- [15] C. Yeh, C. Hsieh, A. S. Suggala, D. I. Inouye, and P. Ravikumar, "How sensitive are sensitivity-based explanations?" *CoRR*, vol. abs/1901.09392, 2019. [Online]. Available: <http://arxiv.org/abs/1901.09392>
- [16] W. Xie, X.-H. Li, Z. Lin, L. K. M. Poon, C. C. Cao, and N. L. Zhang, "Two-stage holistic and contrastive explanation of image classification," 2023.
- [17] P. Chen, N. L. Zhang, T. Liu, L. K. M. Poon, and Z. Chen, "Latent tree models for hierarchical topic detection," *CoRR*, vol. abs/1605.06650, 2016. [Online]. Available: <http://arxiv.org/abs/1605.06650>
- [18] J. Gu, Y. Yang, and V. Tresp, "Understanding individual decisions of cnns via contrastive backpropagation," *CoRR*, vol. abs/1812.02100, 2018. [Online]. Available: <http://arxiv.org/abs/1812.02100>
- [19] S. Bach, A. Binder, G. Montavon, F. Klauschen, K.-R. Müller, and W. Samek, "On pixel-wise explanations for non-linear classifier decisions by layer-wise relevance propagation," *PLOS ONE*, vol. 10, no. 7, pp. 1–46, 07 2015. [Online]. Available: <https://doi.org/10.1371/journal.pone.0130140>
- [20] A. Chattopadhyay, A. Sarkar, P. Howlader, and V. N. Balasubramanian, "Grad-cam++: Generalized gradient-based visual explanations for deep convolutional networks," in *2018 IEEE Winter Conference on Applications of Computer Vision (WACV)*, 2018, pp. 839–847.
- [21] S. Desai and H. G. Ramaswamy, "Ablation-cam: Visual explanations for deep convolutional network via gradient-free localization," in *2020 IEEE Winter Conference on Applications of Computer Vision (WACV)*, 2020, pp. 972–980.
- [22] H. Wang, M. Du, F. Yang, and Z. Zhang, "Score-cam: Improved visual explanations via score-weighted class activation mapping," *CoRR*, vol. abs/1910.01279, 2019. [Online]. Available: <http://arxiv.org/abs/1910.01279>
- [23] P.-T. Jiang, C.-B. Zhang, Q. Hou, M.-M. Cheng, and Y. Wei, "Layercam: Exploring hierarchical class activation maps for localization," *IEEE Transactions on Image Processing*, vol. 30, pp. 5875–5888, 2021.
- [24] J. Adebayo, J. Gilmer, M. Muelly, I. Goodfellow, M. Hardt, and B. Kim, "Sanity checks for saliency maps," in *Proceedings of the 32nd International Conference on Neural Information Processing Systems*, ser. NIPS'18. Red Hook, NY, USA: Curran Associates Inc., 2018, p. 9525–9536.
- [25] N. Kalibhat, K. Narang, H. Firooz, M. Sanjabi, and S. Feizi, "Measuring self-supervised representation quality for downstream classification using discriminative features," 2023.
- [26] S. Krishna, T. Han, A. Gu, J. Pombra, S. Jabbari, S. Wu, and H. Lakkaraju, "The disagreement problem in explainable machine learning: A practitioner's perspective," *CoRR*, vol. abs/2202.01602, 2022. [Online]. Available: <https://arxiv.org/abs/2202.01602>
- [27] K. He, X. Zhang, S. Ren, and J. Sun, "Deep residual learning for image recognition," *CoRR*, vol. abs/1512.03385, 2015. [Online]. Available: <http://arxiv.org/abs/1512.03385>
- [28] Z. Liu, H. Mao, C. Wu, C. Feichtenhofer, T. Darrell, and S. Xie, "A convnet for the 2020s," *CoRR*, vol. abs/2201.03545, 2022. [Online]. Available: <https://arxiv.org/abs/2201.03545>
- [29] G. Huang, Z. Liu, and K. Q. Weinberger, "Densely connected convolutional networks," *CoRR*, vol. abs/1608.06993, 2016. [Online]. Available: <http://arxiv.org/abs/1608.06993>
- [30] J. Deng, W. Dong, R. Socher, L.-J. Li, K. Li, and L. Fei-Fei, "Imagenet: A large-scale hierarchical image database," in *2009 IEEE Conference on Computer Vision and Pattern Recognition*, 2009, pp. 248–255.
- [31] A. Krizhevsky, "Learning multiple layers of features from tiny images," 2009. [Online]. Available: <https://api.semanticscholar.org/CorpusID:18268744>

## APPENDIX

## A. Agreement Score Distributions by Method

To complement the statistical analysis reported in Section V-A, we visualize the distribution of class agreement scores for each saliency method across all tested architectures. These histograms represent the percentage overlap between top-1 and top-2 saliency maps, aggregated over all validation images.

Each plot shows the relative frequency of agreement values (in 5% bins), with a red dashed line marking the 50% threshold used in our Wilcoxon signed-rank test. Distributions heavily concentrated below this line indicate strong class sensitivity, whereas those concentrated above suggest class-insensitive attribution behavior.

We present these distributions for each of the four architectures evaluated in the main paper: VGG, ResNet, ConvNeXt, and DenseNet. For DenseNet, we include two variants: one using the final convolutional layer (`conv2`), and another using the final normalization layer (`norm5`). This dual analysis allows us to visualize how attribution quality shifts with layer selection, supporting our ablation findings in Section V-B.

*a) VGG-19.* VGG serves as a strong baseline for class sensitivity analysis due to its simple, sequential architecture. As the attribution layer activates broadly across many channels, we expect higher top-1/top-2 agreement. The distributions below show that most methods yield class-insensitive explanations, with significant overlap above the 50% threshold.

## Feature Agreement Score Distributions for VGG

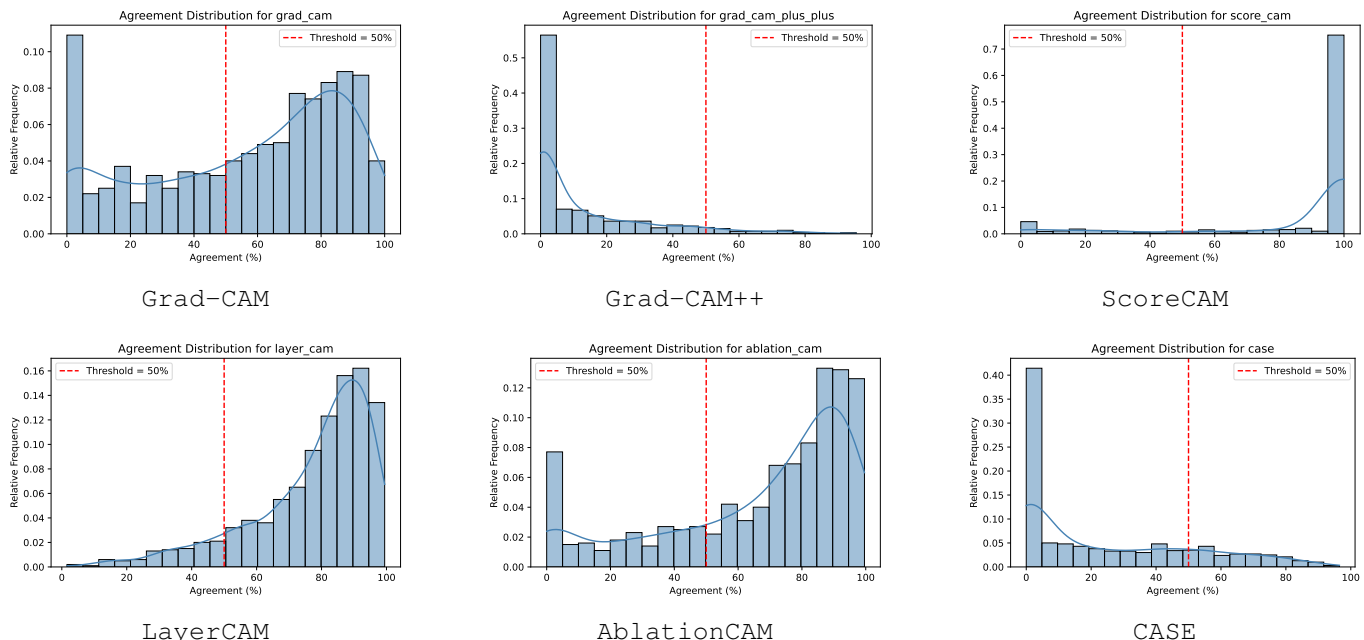


Fig. 7. Agreement score distributions for all saliency methods (VGG). Each histogram shows the distribution of top-5% feature overlap between saliency maps generated for top-1 and top-2 class labels. The red dashed line denotes the 50% threshold used in our Wilcoxon test for class sensitivity.

*b) ResNet-50.* ResNet introduces residual connections that promote feature reuse and broader spatial coverage. These plots reveal that many saliency methods still produce class-indistinct maps, with distributions often centered near or above the 50% threshold. CASE, however, consistently shifts agreement lower, reflecting stronger separation of class-relevant features.

*c) ConvNeXt.* ConvNeXt offers a modern convolutional backbone with enhanced channel mixing and normalization. Despite its design, several methods exhibit high agreement scores across class predictions, indicating limited class specificity. CASE maintains a clear advantage, with distributions skewed leftward below the threshold.

*d) DenseNet-201 (`features.denseblock4.denselayer32.conv2`).* This is the final convolutional layer used in our main experiments. As detailed in Section V-B, it is extremely sparse yet highly class-discriminative. The agreement distributions here confirm that most methods produce low-overlap explanations, consistent with the high class sensitivity reported in RQ1.

*e) DenseNet-201 (`features.norm5`).* This final normalization layer aggregates upstream activations and is located immediately before the classifier. As discussed in our ablation study, this layer activates nearly all channels uniformly. The agreement distributions below reveal that most methods fail to produce class-distinct saliency maps in this setting, highlighting the importance of attribution layer selection.

### Feature Agreement Score Distributions for ResNet

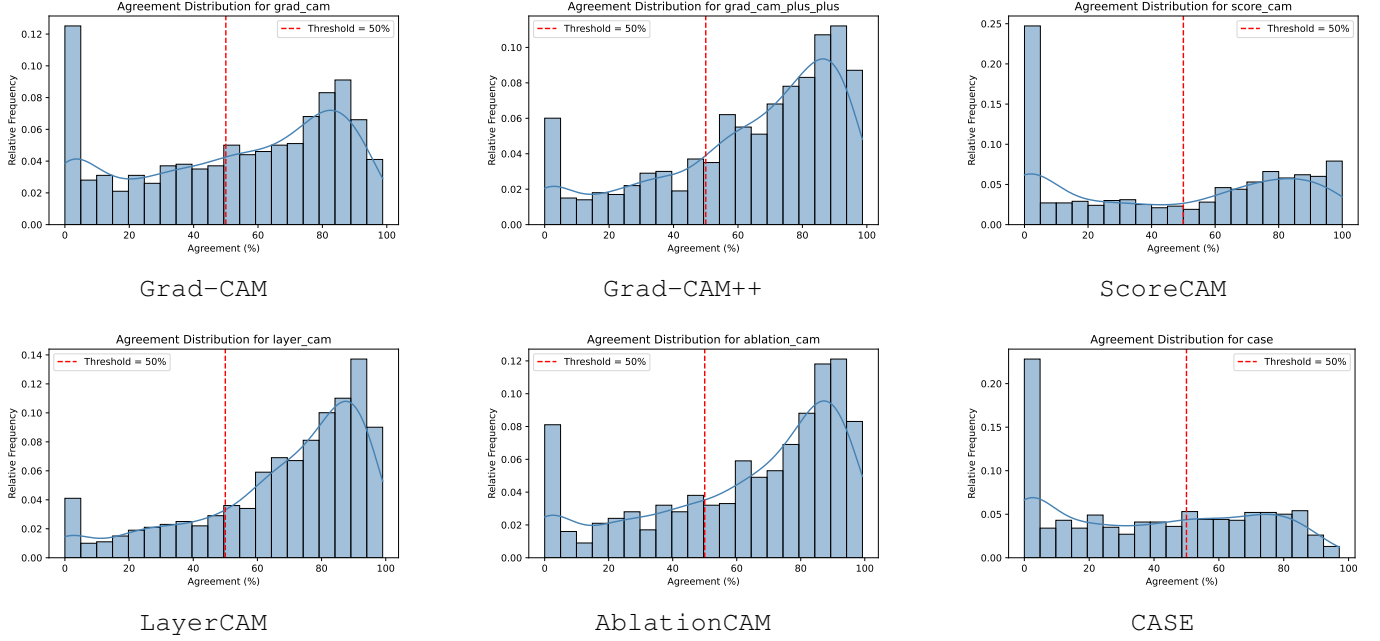


Fig. 8. Agreement score distributions for all saliency methods (ResNet). Each histogram shows the distribution of top-5% feature overlap between saliency maps generated for top-1 and top-2 class labels. The red dashed line denotes the 50% threshold used in our Wilcoxon test for class sensitivity.

### Feature Agreement Score Distributions for ConvNeXt

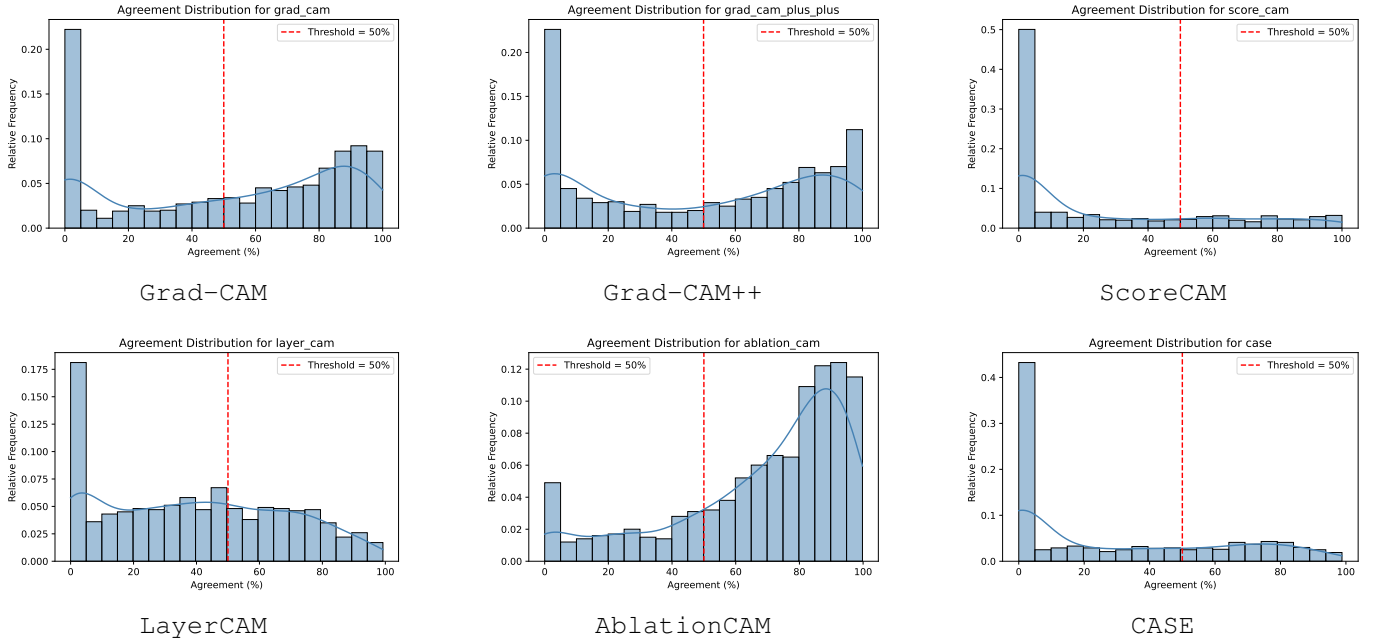


Fig. 9. Agreement score distributions for all saliency methods (ConvNeXt). Each histogram shows the distribution of top-5% feature overlap between saliency maps generated for top-1 and top-2 class labels. The red dashed line denotes the 50% threshold used in our Wilcoxon test for class sensitivity.

### Feature Agreement Score Distributions for DenseNet (Conv)

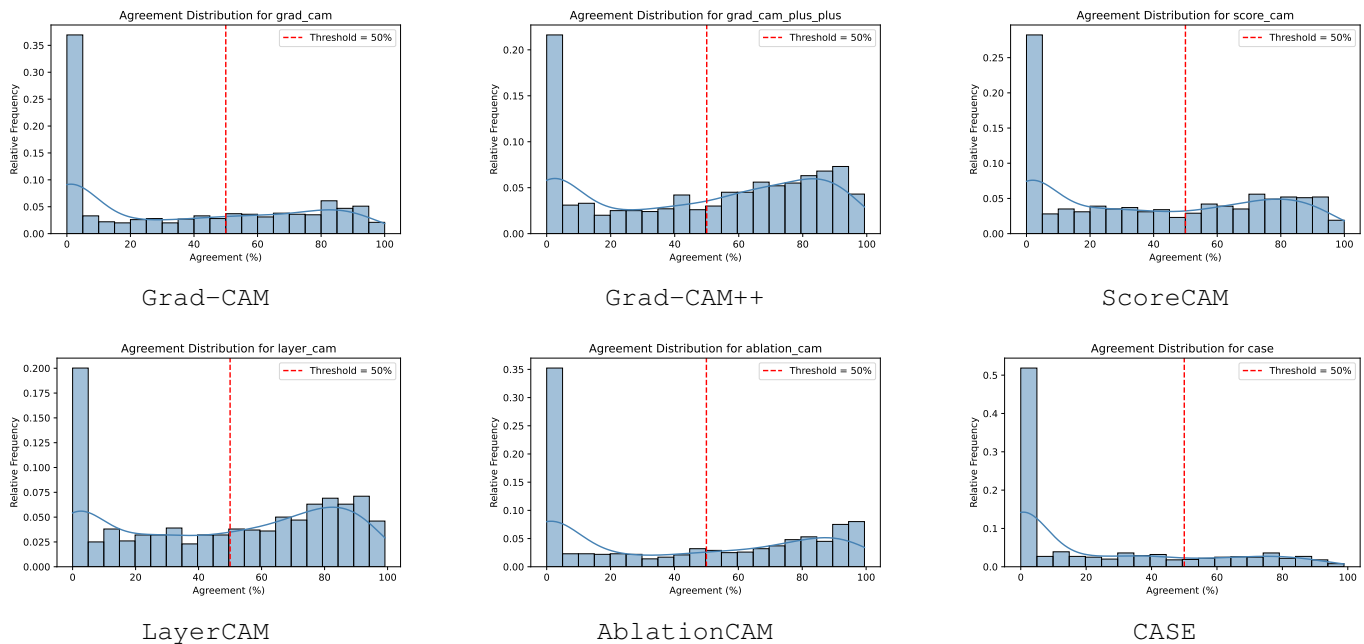


Fig. 10. Agreement score distributions for all saliency methods (DenseNet (Conv)). Each histogram shows the distribution of top-5% feature overlap between saliency maps generated for top-1 and top-2 class labels. The red dashed line denotes the 50% threshold used in our Wilcoxon test for class sensitivity.

### Feature Agreement Score Distributions for DenseNet (norm5)

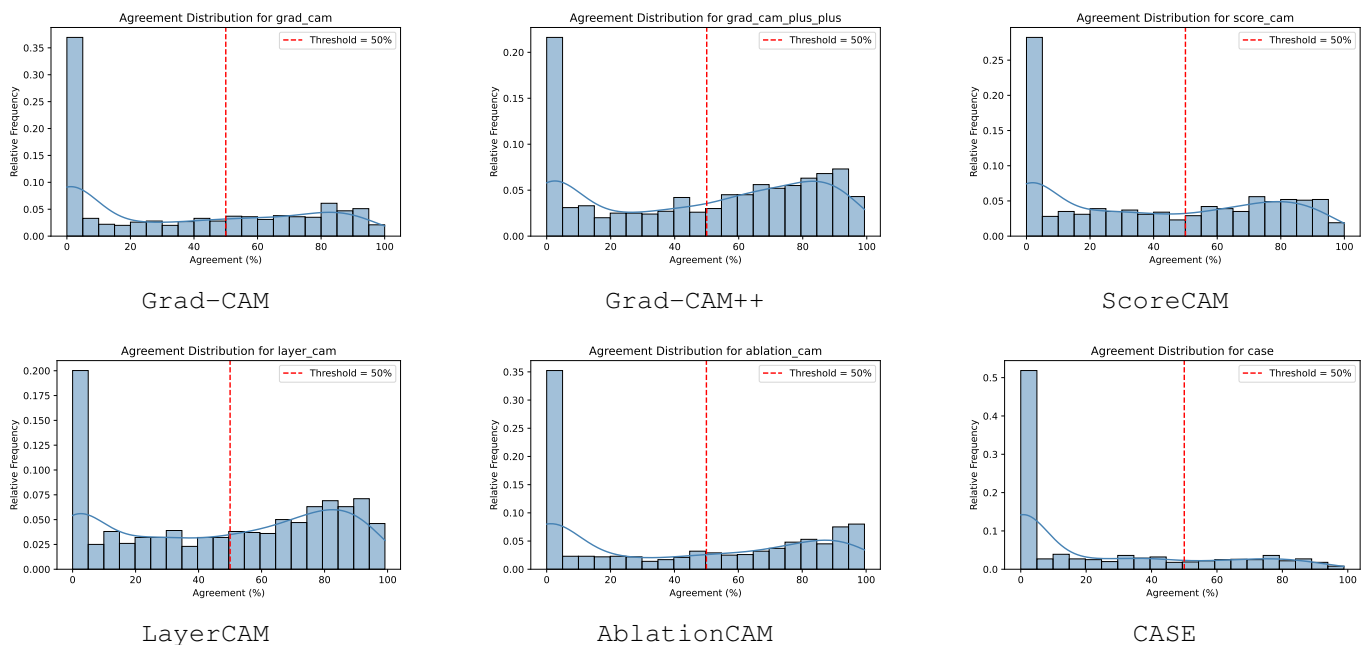


Fig. 11. Agreement score distributions for all saliency methods (DenseNet (Norm5)). Each histogram shows the distribution of top-5% feature overlap between saliency maps generated for top-1 and top-2 class labels. The red dashed line denotes the 50% threshold used in our Wilcoxon test for class sensitivity.